Engineering genetically encoded FRET sensors

BIOCHEMISTRY
including biophysical chemistry & molecular biology

Article

pubs.acs.org/biochemistry

Quantifying Stickiness: Thermodynamic Characterization of Intramolecular Domain Interactions To Guide the Design of Förster Resonance Energy Transfer Sensors

Laurens H. Lindenburg,[†] Mantas Malisauskas,[†] Tari Sips,[†] Lisanne van Oppen,[†] Sjors P. W. Wijnands,[†] Stan F. J. van de Graaf,[‡] and Maarten Merkx*[,†]

[†]Laboratory of Chemical Biology and Institute of Complex Molecular Systems (ICMS), Department of Biomedical Engineering, Eindhoven University of Technology, Eindhoven, The Netherlands

[‡]Tytgat Institute for Liver and Intestinal Research, Department of Gastroenterology & Hepatology, Academic Medical Center, University of Amsterdam, Amsterdam, The Netherlands

Supporting Information

ABSTRACT: The introduction of weak, hydrophobic interactions between fluorescent protein domains (FPs) can substantially increase the dynamic range (DR) of Förster resonance energy transfer (FRET)-based sensor systems. Here we report a comprehensive thermodynamic characterization of the stability of a range of self-associating FRET pairs. A new method is introduced that allows direct quantification of the stability of weak FP interactions by monitoring intramolecular complex formation as a function of urea concentration. The commonly used S208F mutation stabilized intramolecular FP complex formation by 2.0 kCal/mol when studied in an enhanced cyan FP (ECFP)−linker−enhanced yellow FP (EYFP) fusion protein, whereas a significantly weaker interaction was observed for the homologous Cerulean/Citrine FRET pair (ΔG^0_{o-c} = 0.62 kCal/mol). The latter effect could be attributed to two mutations in Cerulean (Y145A and H148D) that destabilize complex formation with Citrine. Systematic analysis of the contribution of residues 125 and 127 at the dimerization interface in mOrange−linker−mCherry fusion proteins yielded a toolbox of new mOrange−mCherry combinations that allowed tuning of their intramolecular interaction from very weak (ΔG^0_{o-c} = −0.39 kCal/mol) to relatively stable (ΔG^0_{o-c} = 2.2 kCal/mol). The effects of these mutations were also studied by monitoring homodimerization of mCherry variants using fluorescence anisotropy. These mutations affected intramolecular and intermolecular domain interactions similarly, although FP interactions were found to be stronger in the latter. The knowledge thus obtained allowed successful construction of a red-shifted variant of the bile acid FRET sensor BAS-1 by replacement of the self-associating Cerulean−Citrine pair by mOrange−mCherry variants with a similar intramolecular affinity. Our findings thus allow a better understanding of the subtle but important role of intramolecular domain interactions in current FRET sensors and help guide the construction of new sensors using modular design strategies.

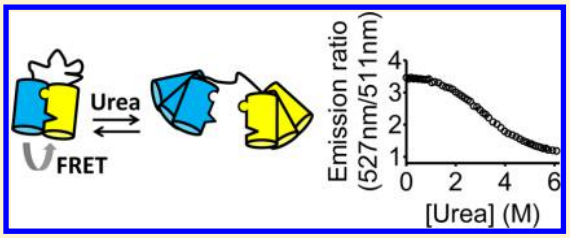

Förster resonance energy transfer (FRET)-based protein sensors are attractive tools to image changes in small molecule concentrations at subcellular resolution. These genetically encoded sensors typically consist of one or more receptor domains, fused between a donor and an acceptor fluorescent protein (FP). The transfer of energy from a donor, such as cyan FP (CFP), to an acceptor, such as yellow FP (YFP), can be modulated through changes in conformation of the receptor domain and is readily detected through a change in the ratio of acceptor to donor emission intensity.[1] Sensors are now available for many different small molecules, as well as a variety of enzyme activities.[2−4] Most FRET sensors developed to date function by tight coupling of the fluorescent domains to the N- and C-termini of the receptor domain, such that changes in receptor conformation are directly transmitted to a change in the FPs' relative distance. Unfortunately, such designs often require time-consuming empirical testing to achieve the best possible response from the sensor.[5] For example, to produce a troponin C-based Ca^{2+} FRET sensor with sufficient dynamic range (DR), 70 different protein variants were purified and characterized in vitro.[6] Furthermore, most FRET sensors developed so far lack modularity. For instance, replacement of CFP/YFP FRET pairs with red-shifted FRET pairs can significantly dampen the DR,[7,8] and even the exchange of ECFP for the highly homologous Cerulean is apparently not always tolerated.[9]

We recently introduced an alternative, rational design strategy for FRET sensor proteins that relies on mutually exclusive domain interactions. In one conformation, the FP pair forms an intramolecular complex, mediated by hydrophobic surface mutations, leading to high FRET efficiency. Addition of ligand renders the second conformation energetically favorable,

Received: April 9, 2014
Revised: August 24, 2014
Published: September 12, 2014

   dx.doi.org/10.1021/bi500433j | *Biochemistry* 2014, 53, 6370−6381

resulting in disruption of the intramolecular FP complex and a substantial decrease in FRET efficiency (Figure 1). Several

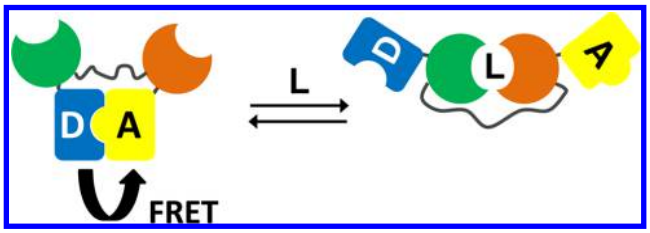

Figure 1. Weakly associating fluorescent domains improve the dynamic range of FRET sensors based on mutually exclusive interactions. Schematic representation of the ligand-dependent equilibrium that exists between two mutually exclusive conformations of a FRET sensor. In absence of ligand (L), donor and acceptor FPs (in blue and yellow) form an intramolecular complex, resulting in high FRET. The ligand induces an interaction between the ligand binding domains (in green and orange) that is mutually exclusive with the intramolecular FP complex, resulting in a large decrease in FRET.

sensors have been explicitly designed based on this concept of mutually exclusive domain interactions, including sensors for protease activity,[10] Zn^{2+},[11,12] Cu^{+},[13] peptides,[14] antibodies,[15] and bile acids.[16] "Sticky" mutations that promote the intramolecular interaction between FP domains, such as S208F on ECFP and EYFP, play a crucial role in all of these sensors, as in their absence the sensors show no or only a weak response. The sensors' modular design not only ensures robust changes in energy transfer efficiency but was also shown to allow easy exchange of the original CFP and YFP output domains by a newly developed FRET pair of self-associating variants of mOrange and mCherry carrying the R125I mutation.[12]

Although the FRET sensors discussed above greatly benefited from the introduction of interaction-promoting mutations on the fluorescent domains, a sensor's architecture must be carefully considered in deciding whether the probe's response would stand to benefit from this approach. In fact, even without deliberate introduction of self-association promoting mutations, some highly optimized sensors may already depend on intramolecular FP domain interactions.[8,17] Introduction of both dimerizing (S208F and V224L) and monomerizing (A206K) mutations in highly optimized FRET sensors for Ca^{2+} resulted in attenuation of their DR, suggesting that the level of FP complex formation needs to be carefully balanced for optimal sensor performance.[17] Similarly, introduction of monomerizing mutations in two different FRET sensors for kinase activity had a detrimental effect on their DR, emphasizing the importance of intramolecular FP complex formation in these sensors' mechanism of action.[8]

Direct quantification of intramolecular FP domain interactions would help in understanding the equilibria at play in these single chain FRET sensors and could guide future FRET sensor design. Here we present an in-depth thermodynamic characterization of a range of self-associating CFP/YFP and mOrange/mCherry-based FRET pairs. Urea titration is introduced as a new approach to quantify the stability of intramolecular domain interactions. By systematically studying the contribution of mutations at the critical 125/127 interface positions of mOrange and mCherry, a toolbox of FRET pairs is developed covering a broad range of interaction strengths. We demonstrate its utility by constructing the first red-shifted FRET sensor for intracellular bile acids. The findings reported in this study help to clarify the influence of FP domains' interactions in current FRET-sensor performance and provide a framework for the more rational design of new FRET sensor systems.

EXPERIMENTAL PROCEDURES

Cloning of Protein Expression Constructs. The pET28a-based bacterial expression constructs for ECFP-L9-EYFP, ECFP*-L9-EYFP*, and Cer*-L9-Cit* (where * represents the combination of S208F and V224L on the fluorescent domain) were described previously.[11,18] In the latter construct, homology between the DNA sequences encoding Cerulean and Citrine hindered efficient site-directed mutagenesis so that a more complex cloning effort to obtain pET28a-Cer*(A145Y/D148H)-L9-Cit* was required. Briefly, circular polymerase extension cloning (CPEC)[19] was used to generate the construct from a synthetic gene in which the Cerulean and Citrine DNA sequences had been diversified as much as possible (Figure S1, Supporting Information). Primers to generate the A145Y and D148H mutations on Cerulean are listed in Table S1, Supporting Information. To generate mutations at amino acid positions 125 and 127 (numbering relative to DsRed) of mOrange and mCherry in the vector encoding the red-shifted FRET construct, pET28a−mOrange−linker−mCherry,[12] site-directed mutagenesis was used, together with the primers listed in Table S1. Single domain mCherry constructs were generated through a one-step site-directed deletion mutagenesis of the mOrange and linker domains of the red protease constructs, as previously described.[12] The pET28a-redBAS constructs were also generated used CPEC,[19] with pET28a-BAS-1,[16] pGen2.1-mOrange2(R125I)−linker−mCherry(R125I)[12] and pET28a as input plasmids. Second, a C-terminal Strep-tag was introduced by site-directed mutagenesis, with primers FXR_Strep_F and FXR_Strep_R, resulting in pET28a-redBAS-1 (Figure S2, Supporting Information). At this point, the T127V mutations were introduced by CPEC too. PCR fragments were generated with various combinations of the primers RCS_mCh_T127V_F, RCS_mCh_T127V_R, RCS_mO_T127V_F and RCS_mO_T127V_R, together with FXR_Strep_F and FXR_Strep_R (Table S1). In order to create redBAS-0, CPEC was used to introduce the I125R mutations in mOrange and mCherry in pET28a-redBAS-1. Primers RCS_mOr2_I125R_F and RCS_mCh_I125R_R were used in a PCR reaction to create a fragment spanning the two 125 positions of both fluorescent domains. Primers RCS_mOr2_I125R_R and RCS_mCh_I125R_F allowed amplification of the vector backbone and sequence to the 5′-side of position 125 in mOrange2 and to the 3′-side of the 125 position in mCherry. These two fragments, whose ends were homologous, were then recombined by CPEC. All constructs were confirmed by DNA sequencing (Baseclear, Leiden) prior to use.

Protein Expression and Purification. *Escherichia coli* BL21(DE3) (Novagen) was transformed with the various pET28a expression constructs and single colonies of the transformants were used to inoculate 5 mL of lysogeny broth (LB) starter cultures containing 30 μg/mL kanamycine, which in turn were used to inoculate 500 mL (all constructs except redBAS-1) or 2 L (redBAS-1) of LB cultures. Protein expression was induced at an OD_{600} of 0.6 through addition of 0.1 mM IPTG. Expression was carried out overnight at 25

dx.doi.org/10.1021/bi500433j | *Biochemistry* 2014, 53, 6370−6381

°C. Cells were harvested by centrifugation and lysed with BugBuster (Novagen), and the soluble fractions, obtained through centrifugation at 40000*g*, were loaded onto a Ni-NTA column (HisBind resin, Novagen), washed, and eluted following the manufacturer's instructions, exploiting the N-terminal polyHis-tag carried by all constructs used in this study. Constructs encoding only a single mCherry domain were buffer exchanged to 50 mM Tris-HCl (pH 8), 100 mM NaCl and stored in aliquots at −80 °C. Size exclusion chromatography (SEC) was used to purify full length ECFP*-L9-EYFP*, Cerulean*-L9-Citrine*, mOr(I125/T127)−linker−mCh(I125/T127), mOr(I125/T127)−linker−mCh(I125/V127), mOr(I125/V127)−linker−mCh(I125/T127), and mOr(I125/V127)−linker−mCh(I125/V127), separating them from undesired C-terminally truncated products. The SEC column (HiPrep 26/60 Sephacryl S-200 HR, GE Healthcare) was equilibrated with 100 mM NaCl, 50 mM Tris-HCl (pH 8). Protein SEC fractions were analyzed for correct size and purity by SDS-PAGE, pooled, and concentrated using 10 kDa MWCO centrifugation tubes (Millipore). The mOrange−linker−mCherry constructs not mentioned above, Cer*-(A145Y/D148H)-L9-Cit*, and the redBAS variants were purified through streptactin chromatography following Ni-NTA purification, instead of by SEC. These proteins carried a C-terminal Strep-tag II, allowing purification of full length protein, following the streptactin resin manufacturer's instructions (IBA GmbH). The redBAS-0 variant was found to be of insufficient purity after streptactin chromatography and was therefore subjected to an additional SEC step, following the procedure described above. All buffers (except BugBuster) used for the purification of the redBAS variants additionally contained 0.5 mM TCEP, as it was found that redBAS-1 was only functional when purified under reducing conditions. Protein concentrations were determined by absorbance using the published extinction coefficients for EYFP (80400 M^{-1} cm^{-1} at 515 nm[20]), Citrine (77000 M^{-1} cm^{-1} at 516 nm[21]), or mCherry (72000 M^{-1} cm^{-1} at 587 nm[22]).

Urea Titration Experiments. A stock solution of 10 M urea in 50 mM Tris-HCl (pH 8), 100 mM NaCl, and 10% (v/v) glycerol was prepared by dissolving urea in preheated buffer in a flask suspended in a bath of hot water that was allowed to cool slowly, with continuous stirring of the urea solution. Because of the known instability of urea in solution, this solution was always prepared on the day of use. Protein variants were dissolved at 1.5 μM (CFP/YFP variants) or 0.5 μM (mOrange/mCherry variants) in a buffer consisting of 50 mM Tris-HCl (pH 8), 100 mM NaCl and 10% (v/v) glycerol in quartz cuvettes with 1 cm path length, at 20 °C. The urea concentration was increased by stepwise addition of 10 M urea, and an emission spectrum was measured at each concentration of urea, either between 450 and 600 nm (ECFP/EYFP pair and derivatives) or between 550 and 650 nm (mOrange/mCherry pair), and either through excitation with 420 nm (ECFP/EYFP) or 520 nm (mOrange/mCherry) light. For the ECFP/EYFP and Cerulean/Citrine constructs, the acceptor's peak intensity (at 527 nm) was corrected for the effect of sample dilution by dividing this intensity by the intensity at 511 nm. The latter wavelength was determined to be an isosbestic point within the ECFP/EYFP and Cerulean/Citrine spectra. The mOrange/mCherry construct spectra were processed by dividing the donor's peak intensity (at 562 nm) by the acceptor's peak intensity (at 610 nm).

Protease-Based Screening for FRET in mOrange/mCherry FRET Pairs. As previously described,[10,12] to cleave the linker between the mOrange−linker−mCherry constructs, 0.006 U Protease K (Sigma) was added to the 2 mL solutions of FRET sensor protein. Emission spectra that were monitored over time confirmed cleavage to be complete after ∼15 min, as ascertained by the reduction in the emission ratio.

HomoFRET-Induced Fluorescence Depolarization Assay. The mCherry variants' anisotropy was monitored at increasing protein concentration, as described previously.[12] Briefly, measurements were performed in 50 mM Tris-HCl (pH 8), 100 mM NaCl and 1 mg/mL BSA, at 25 °C with an excitation wavelength of 560 nm, a 20 nm excitation slit width, a 5 nm emission slit width, while monitoring emission between 595 and 615 nm, using a Cary Eclipse fluorescence spectrophotometer (Varian). Data were fit to the same binding model described previously,[12,23] using a single high anisotropy value for the monomeric states and a single low anisotropy value for the dimeric states for all data sets. Great care was taken to ensure measurement conditions such as temperature and buffer were kept as constant as possible as even small deviations had a significant effect on absolute anisotropy values.

Relating Intermolecular Dimerization Affinity to Intramolecular Dimer Stability. As explained in the Results, the experimentally determined values for the intramolecular equilibria can be related to the experimentally determined values for the intermolecular dimer $K_{d,inter}$ by an effective concentration (C_{eff}) term, according to eq 1.

$$K_{d,intra} = \frac{K_{d,inter}}{C_{eff}} \tag{1}$$

The $K_{d,intra}$ can then be used to calculate the Gibbs free energy associated with transition from the closed to opened state, applying eq 2.

$$\Delta G^0_{o-c} = -RT \ln(K_{d,intra}) \tag{2}$$

Characterization of redBAS Variants. Fluorescence measurements were done using 0.2 μM protein concentration, in measurement buffer containing 50 mM Tris-HCl (pH 8), 100 mM NaCl, 1 mM DTT in a 1 × 1 cm cuvette, at 25 °C. A fluorescence spectrophotometer (Varian Eclipse) was set to excite samples at 520 nm and to record emission between 530 and 650 nm. Stock solutions of cholic acid (5 mM) and chenodeoxycholic acid (25 mM) (both from Sigma-Aldrich) were prepared in measurement buffer and added stepwise to increase the bile acid concentration. To determine dissociation constants (K_d's) the emission ratio (R, 562 nm/610 nm) was fit as a function of bile acid concentration ([BA]) using eq 3.

$$R = \frac{P_1[\mathrm{BA}]}{K_d + [\mathrm{BA}]} + P_2 \tag{3}$$

Here P_1 is the difference in ratio between the BA-saturated and BA-depleted states, and P_2 is the ratio in the BA-depleted state of the sensor.

RESULTS

Urea Titrations Can Be Used To Quantify the Strength of Intramolecular Domain−Domain Interactions. To quantify the stability of the interaction between ECFP and EYFP mediated by the previously reported[10,24] combination of the S208F and V224L mutations (henceforth denoted by *), the amount of FRET was monitored as a function of urea

concentration using a fusion construct consisting of the two fluorescent domains connected by a linker containing nine GGSGGS repeats (ECFP*-L9-EYFP*).[10,18] This approach is analogous to a classical equilibrium unfolding experiment where single domains are exposed to increasing concentrations of denaturant. It is important to note that FPs are known to be stable to high urea concentrations.[25] Previously, we and others have typically reported changes in FRET through the acceptor/donor emission ratio. However, a recent report by Krężel and co-workers showed that this approach can sometimes result in systematic errors in the interpretation of binding data,[26] in particular when dividing the intensity that changes the least by the intensity that changes the most. We therefore choose to report changes in FRET by monitoring the intensity at the acceptor's peak, divided by the intensity at 511 nm, which is the isosbestic point for ECFP-EYFP spectra (Figure S3). In this way, changes in complex formation can be monitored more accurately by monitoring the fluorescence intensity at a single wavelength, while still correcting for changes in the absolute concentration of the fluorescent protein. ECFP*-L9-EYFP* displayed an emission ratio of ~3.5 under "native" conditions (pH 8, 20 °C) (Figure 2A). Addition of urea resulted in a decrease in emission ratio, indicating a decrease in FRET due to disruption of the intramolecular complex between ECFP* and EYFP*. In contrast, the same fusion construct lacking the S208F/V224L mutations (ECFP-L9-EYFP) displayed a much lower emission ratio under native (0 M urea) conditions (Figure 2B). We have previously shown that the amount of FRET in ECFP-L9-EYFP can be quantitatively understood based on the random coil behavior of the linker and in addition used SEC and fluorescence anisotropy to show the absence of an intramolecular domain interaction between the wild-type ECFP and EYFP.[10,18] The small decrease in emission ratio observed upon addition of urea is therefore not due to the disruption of a residual interaction between the two fluorescent domains but results from the effect of urea on the conformational distribution of the long flexible linker. In water, polyserine/glycine chains form relatively compact, random coil-like structures due to intrachain hydrogen bonds that result in loops within the chain.[18,27] Previous work on isolated polyserine/glycine peptides has shown that denaturants disrupt those bonds, resulting in an increase of the end-to-end distance distribution[28,29] and thus a lower efficiency of energy transfer between ECFP and EYFP.

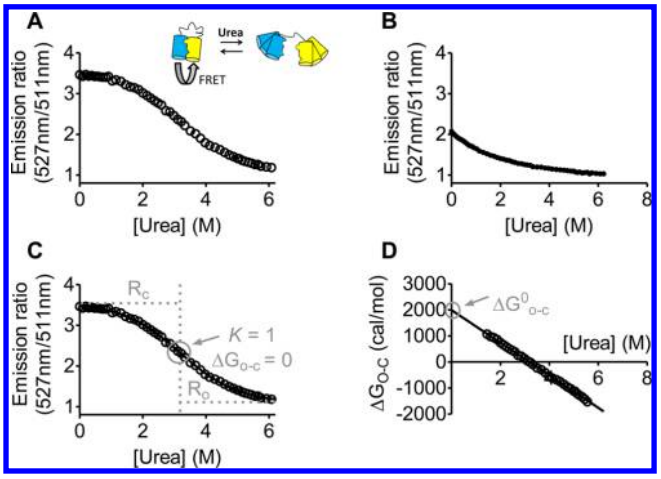

Figure 2. Use of urea titrations to establish the stability of the intramolecular dimer interface in ECFP*-L9-EYFP*. Fluorescence emission ratio of ECFP*-L9-EYFP* (A) or ECFP-L9-EYFP (B) monitored as a function of urea concentration. (C) The data for ECFP*-L9-EYFP* were fit to a Boltzmann distribution, assuming a transition between closed and opened sensor. The emission ratio corresponding to completely closed sensor (R_c) and completely opened sensor (R_o) are indicated in gray. Also indicated in gray is the titration midpoint (x_0) at which there is an equal amount of closed and opened sensor at equilibrium, so that the equilibrium constant (K) is equal to 1 and the Gibbs free energy (ΔG_{o-c}) is equal to 0. (D) Plot showing the linear correlation between the urea concentration and the Gibbs free energy associated with transition from the closed to opened state. Data were fit to a linear model and extrapolated to 0 M urea, providing the standard Gibbs free energy of the complex under native conditions (ΔG^0_{o-c}), indicated by the gray circle at the intersection of the fit with the Y-axis. Urea titrations were carried out using 1.5 μM protein, in 50 mM Tris-HCl (pH 8), 100 mM NaCl, 10% (v/v) glycerol, at 20 °C.

The increased amount of FRET seen in ECFP*-L9-EYFP* could also partially result from intermolecular interactions between fluorescent domains of two different proteins. However, formation of such oligomeric complexes would also result in homoFRET between, e.g., two EYFP acceptor domains, which can be assessed by measuring the fluorescence anisotropy of the acceptor domain, since homoFRET would lead to a strong decrease in fluorescence polarization. The acceptor anisotropy in ECFP*-L9-EYFP* and other variants with sticky fluorescent domains (see below) was found to be similar to previously reported values for (nonsticky) EYFP and independent of protein concentration (Table S2). These results confirm that the increased FRET was solely due to an intramolecular interaction between the donor and acceptor fluorescent domain and inconsistent with the formation of intermolecular domain interactions, at least at the low micromolar concentrations that we used in this study.

The emission ratio for construct ECFP*-L9-EYFP* displayed a sigmoidal dependence on urea concentration (Figure 2A) indicating a two-state equilibrium between sensor in the closed and in the opened state (Figure 2A, inset). The sigmoidal curve was fit to a Boltzmann distribution using eq 4 (Figure 2C),

$$R_x = R_o + \frac{R_c - R_o}{1 + e^{\frac{x - x_0}{dx}}} \quad (4)$$

where the emission ratio at each concentration of urea (R_x) depends on the emission ratio in the closed state of the sensor (R_c), the ratio in the opened state (R_o), the urea concentration (x), the point of inflection of the curve where precisely 50% of the sensor remains in the closed state (x_0), and the slope of the curve at the inflection point (dx). Next, the equilibrium constants at each concentration of urea (K_x) were calculated using eq 5,

$$K_x = \frac{(R_c - R_x)}{(R_x - R_o)} \quad (5)$$

where R_x is the emission ratio observed at a particular concentration of urea. From the equilibrium constants, the Gibbs free energy associated with the transition from closed to opened sensor at any particular concentration of urea (ΔG^x_{o-c}) was calculated using eq 6,

$$\Delta G^x_{o-c} = -RT \ln(K_x) \quad (6)$$

dx.doi.org/10.1021/bi500433j | Biochemistry 2014, 53, 6370−6381

Table 1. Thermodynamic Parameters of Urea-Induced Dissociation of the CFP-YFP Intramolecular Dimer

FP pair	R_c ± SE	R_o ± SE	x_0 (M) ± SE	m (kcal/mol/M) ± SE	ΔG^0_{o-c} (kcal/mol) ± SE
ECFP*-L9-EYFP*	3.56 ± 0.01	1.09 ± 0.01	3.18 ± 0.01	−0.624 ± 0.003	1.99 ± 0.01
Cer*-L9-Cit*	3.91 ± 0.1	0.891 ± 0.01	1.44 ± 0.1	−0.429 ± 0.0071	0.62 ± 0.02
Cer*(A145Y/D148H)-L9-Cit*	3.80 ± 0.03	0.981 ± 0.02	3.25 ± 0.03	−0.547 ± 0.007	1.81 ± 0.03

where R is the gas constant (1.987 cal/mol/deg) and T is the temperature (293.15 K). In analogy to classical domain unfolding studies, changes in ΔG_{o-c} displayed a negative linear correlation to increasing urea concentration (Figure 2D). This trend was fit to eq 7,

$$\Delta G^x_{o-c} = \Delta G^0_{o-c} + mx \quad (7)$$

where ΔG^0_{o-c} represents the extrapolation of ΔG_{o-c} to 0 M urea, indicating the stability of the intramolecular FP interaction under native conditions, ΔG^0_{o-c} = 2.0 kcal/mol (Figure 2D, Table 1). The slope of the urea-ΔG_{c-o} relationship, m, was found to be −0.62 kcal/mol/M (Table 1). Parameter m is known to correlate with the difference in solvent-exposed hydrophobic area between the folded and unfolded state. The small value of m found here is thus consistent with the exposure of a relatively small solvent-excluded contact area and certainly not indicative of global domain unfolding.[30,31]

Cerulean-Specific Mutations Attenuate Intramolecular FP Interactions. Cerulean and Citrine are frequently used in modern FRET sensors as these FPs have optimized properties relative to their parent proteins ECFP and EYFP respectively, including improved brightness, photostability, and, for Citrine, decreased pH sensitivity.[21,32] Having established the suitability of urea-based analysis to determine the stability of the intramolecular donor−acceptor FP complex, we next tested the effect of mutations S208F and V224L on the Cerulean and Citrine donor/acceptor pair. Cer*-L9-Cit* again displayed a high emission ratio under native conditions and showed a clear transition to a low FRET state upon addition of increasing concentrations of urea (Figure 3A). However, the transition took place at lower urea concentrations than seen with ECFP*-L9-EYFP* and started immediately upon addition of urea. Analysis of these data revealed that Cer*-L9-Cit* displayed a stability of 0.62 kcal/mol under native conditions. Although the lack of a stable plateau phase at lower urea concentrations increased the uncertainty in the determination of R_c and consequently ΔG^0_{o-c}, it is nonetheless clear that Cerulean- and/or Citrine-specific mutations have a substantial effect on intramolecular FP interaction strength.

The decreased stability seen for the Cerulean−Citrine complex may be due to mutations on either one of these improved FP variants. Mutations Q69M in Citrine and S72A in Cerulean are buried inside the beta-barrel in the vicinity of the chromophore and are thus unlikely to affect the FPs' protein−protein interactions. The mutations Y145A and H148D in Cerulean on the other hand are located along the seventh beta-strand of Cerulean, adjacent to the 10th strand containing the S208F residue that is required for the intramolecular dimerization (Figure 3B). In ECFP, H148 is oriented in parallel to the FP surface, but in Cerulean, the D148 side chain is pointing out into the solvent[33] (Figure 3B). The presence of the negatively charged side group could lead to destabilization of the intramolecular domain interaction. Furthermore, in ECFP, Y145 points out into the solvent, whereas in Cerulean, A145 has a tendency to point into the protein core.[33] The presence of the hydrophobic side group of tyrosine at the surface of ECFP may further stabilize hydrophobic interactions. Indeed, a clear increase in stability was observed (to 1.8 kcal/mol) in the construct Cer*(A145Y/D148H)-L9-Cit* (Figure 3A, Table 1), confirming the effect of these mutations on the intramolecular dimer stability. Nevertheless, despite the relatively weak interaction between the Cerulean* and Citrine* domains, these FPs have been successfully applied in a range of FRET sensors,[11,16,34] suggesting that a strong intramolecular interaction is not required to yield FRET sensors with a high DR.

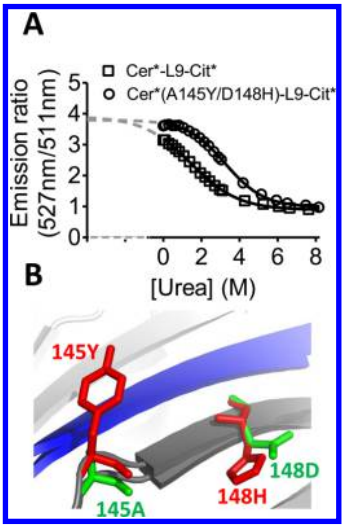

Figure 3. The Cerulean−Citrine intramolecular interface is weaker, due to surface mutations on Cerulean. (A) Fluorescence emission ratio monitored as a function of urea concentration for Cer*-L9-Cit* and Cer*(A145Y/D148H)-L9-Cit*. Curves were fit to a Boltzmann distribution, assuming a transition between closed and opened state. Urea titrations were carried out using 1.5 μM protein, in 50 mM Tris-HCl (pH 8), 100 mM NaCl, 10% (v/v) glycerol, at 20 °C. (B) Detail from an alignment of crystal structures for Cerulean (green; 2WSO) and ECFP (red; 2WSN) showing that residue positions 145 and 148 are in close proximity to strand 10 (colored blue), mutations which are known to be crucial in either forming (Q204F, S208F) or disrupting (A206K) a stable dimeric interface. In ECFP, the hydrophobic side group of 145Y (red) clearly points out toward the hydrophobic interface, but in Cerulean the corresponding 145A (green) is buried in the beta-barrel. Also, in ECFP, 148H (red) is oriented parallel to the protein surface, while in Cerulean, 148D (green) points out into the solvent. For clarity, the alternative "B" position of residue 145 is not shown.

Characterization and Further Tuning of Self-Associating Variants of mOrange and mCherry. Red-shifted FRET pairs such as mOrange/mCherry from the mFruit series are useful complements to the existing CFP/YFP-based variants, yet FRET sensors employing this pair tend to suffer from poor DR, hampering their application in multiparameter imaging.[7,8] We recently discovered that reversion of the I125R mutation, originally carried out to break the mFruits' ancestral DsRed tetramer, was sufficient to bring about intramolecular dimerization between mOrange and mCherry and provided a suitable level of stability to function in the context of a red-

dx.doi.org/10.1021/bi500433j | Biochemistry 2014, 53, 6370−6381

shifted FRET sensor for Zn^{2+}, redCALWY-1.[12] The addition of the T127V mutation, another reversion to the DsRed original was found to further enhance the stability of the interaction. Again, as with the CFP/YFP constructs we confirmed the absence of intermolecular domain interactions by measuring the fluorescence anisotropy of the mCherry at two different protein concentrations for all mOrange−linker−mCherry constructs (Table S3, Supporting Information). To quantify the contributions of both mutations to the stability of the intramolecular FP complex, urea titrations were performed using mOrange−linker−mCherry constructs.[12] For the mOrange/mCherry FRET pair, we chose to analyze the changes in FRET as the donor's peak intensity (at 562 nm) divided by the acceptor's peak intensity (at 610 nm). In this way, the relatively constant mCherry signal served to normalize the more responsive donor intensity.[26] Note that this analysis means low emission ratios are indicative of a higher degree of FRET than are high emission ratios. As expected, a construct bearing the monomeric versions of mOrange and mCherry (mOr(R125/T127)−linker−mCh(R125/T127)) displayed a high starting emission ratio (1.9), indicating a lack of intramolecular interaction between the wild-type fluorescent domains (Figure 4). Addition of urea led to a small increase in the emission ratio,

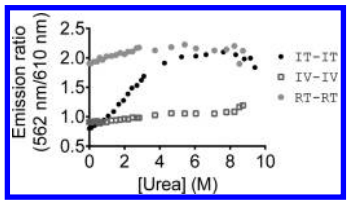

Figure 4. Urea-induced dissociation of the intramolecular mOrange−mCherry dimers. The fluorescence emission ratio was monitored as a function of urea concentration for the wildtype construct (mOr(R125/T127)−linker−mCh(R125/T127)), for mOr(I125/T127)−linker−mCh(I125/T127) and for mOr(I125/V127)−linker−mCh(I125/V127). Urea titrations were carried out using 0.5 μM protein, in 50 mM Tris-HCl (pH 8), 100 mM NaCl, 10% (v/v) glycerol, at 20 °C.

an observation consistent with the previously noted linker stiffening effect of urea. In contrast, constructs mOr(I125/T127)−linker−mCh(I125/T127) and mOr(I125/V127)−linker−mCh(I125/V127) displayed much lower emission ratios of 0.81 and 0.91, indicating FRET due to intramolecular association of the fluorescent domains (Figure 4). Construct mOr(I125/T127)−linker−mCh(I125/T127) showed an immediate increase in emission ratio upon urea addition, reaching the completely opened state at 3 M urea (Figure 4). In contrast, the mOr(I125/V127)−linker−mCh(I125/V127) construct maintained its low emission ratio even at the highest assayable concentrations of urea (Figure 4).

To allow further tuning of the interaction between the fluorescent domains and to better understand the contribution of individual amino acid mutations, the effect of other mutations at positions 125 and 127 was investigated (Figure 5A). Replacement of the positively charged arginine with the hydrophobic isoleucine at the 125 position of both mOrange and mCherry had been found to be sufficient for the formation of an intramolecular association.[12] However, it was unclear whether this effect was due to an increased hydrophobic interaction or due to removal of Coulomb repulsion. To test whether removal of Coulomb repulsion was sufficient to allow complex formation, alanine was introduced at position 125 alone (generating mOr(A125/T127)−linker−mCh(A125/T127)), at both positions 125 and 127 (mOr(A125/A127)−linker−mCh(A125/A127)) or at position 125 in combination with valine at position 127 (mOr(A125/V127)−linker−mCh(A125/V127)). Constructs mOr(A125/T127)−linker−mCh(A125/T127) and (mOr(A125/A127)−linker−mCh(A125/A127) had high emission ratios (2.1 and 1.9, respectively, Figure 5B), similar to the wild-type construct (2.0, Figure 5B,C), consistent with the absence of intramolecular domain interactions. Construct mOr(A125/V127)−linker−mCh(A125/V127), displayed a high, albeit slightly decreased emission ratio relative to wild-type (1.4, Figure 5B). Proteolytic cleavage of the linker in the latter variant resulted in a higher ratio (2.0, Figure 5D), comparable to mOr(R125/T127)−linker−mCh(R125/T127) after cleavage (2.3, Figure 5C). It seemed therefore that removal of Coulomb repulsion alone was insufficient to generate a stable intramolecular dimer. Surprisingly, introduction of the hydrophobic tyrosine at position 127 did not result in complex formation; construct mOr(I125/Y127)−linker−mCh(I125/Y127) displayed a high emission ratio (2.2, Figure 5B) presumably because the bulky aromatic ring of tyrosine sterically hindered the complex formation otherwise mediated by the isoleucines at position 125. Leucine, with its alternatively branched β-carbon, is often considered slightly less hydrophobic than isoleucine and thus was tested as a subtle way to tune the interaction stability. Interestingly, mOr(L125/T127)−linker−mCh(L125/T127) failed to form a complex (ratio 2.4, Figure 5B). Only after the introduction of an additional hydrophobic side group, valine at position 127, was FP complex formation restored (mOr(L125/V127)−linker−mCh(L125/V127), ratio 0.59). Upon proteolytic cleavage of the peptide linker, the mOr(L125/V127)−linker−mCh(L125/V127) emission ratio increased to 1.6 (Figure 5E), confirming that the low emission ratio was due to intramolecular complex formation. Construct mOr(I125/A127)−linker−mCh(I125/A127) was tested in an effort to subtly increase the interaction strength compared to mOr(I125/T127)−linker−mCh(I125/T127). As expected, mOr(I125/A127)−linker−mCh(I125/A127) formed an intramolecular complex displaying a ratio of 0.60 (Figure 5B), which again was increased to a wild-type-like level (1.8) upon cleavage of the linker (Figure 5F).

The stability of the intramolecular complexes in mOr(L125/V127)−linker−mCh(L125/V127), mOr(I125/A127)−linker−mCh(I125/A127) and mOr(A125/V127)−linker−mCh(A125/V127) were quantified using urea titrations. For comparison, mOr(I125/V127)−linker−mCh(I125/T127) and mOr(I125/T127)−linker−mCh(I125/V127), two constructs previously shown to form complexes of intermediate strength[12] were also studied (Figure 6A). Under native conditions, three different emission ratio regimes could be discerned: a low emission ratio of around 0.6 (mOr(L125/V127)−linker−mCh(L125/V127), mOr(I125/A127)−linker−mCh(I125/A127), mOr(I125/V127)−linker−mCh(I125/T127) and mOr(I125/T127)−linker−mCh(I125/V127)), an intermediate ratio of around 0.8 (mOr(I125/T127)−linker−mCh(I125/T127)), and a high emission ratio of around 1.5 (mOr(A125/V127)−linker−mCh(A125/V127)) (Figure 6A). The three regimes reflected three different stability levels, with the low emission ratio group possessing an interaction of sufficient strength to ensure completely closed constructs, the intermediate construct possessing a weaker interaction so that a significant fraction of molecules was in the opened state at 0

dx.doi.org/10.1021/bi500433j | Biochemistry 2014, 53, 6370−6381

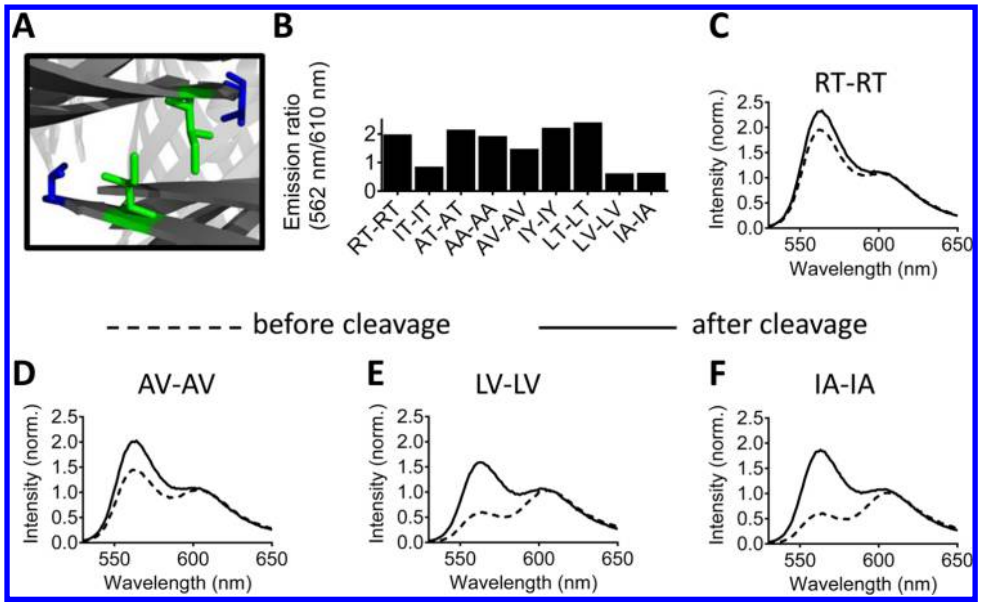

Figure 5. Surveying alternative mutations at positions 125 and 127 capable of mediating a hydrophobic intramolecular interaction between mOrange and mCherry. (A) Detail from the DsRed crystal structure, showing the hydrophobic AB interface. Residue I125 is highlighted in green, while residue V127 is in blue. (B) Donor to acceptor emission ratio (emission at 562 nm/emission at 610 nm) measured for different combinations of mutations. Labels indicate mutations present at positions 125 and 127 of both mOrange and mCherry, respectively, using the single-letter amino acid code. IT-IT is shown for purposes of comparison and is obtained from ref 12. (C) Emission spectra measured before and after proteolytic cleavage of wild-type construct mOr(R125/T127)−linker−mCh(R125/T127). (D−F) Emission spectra measured before and after linker cleavage for those variants that appeared to form a complex before cleavage. Measurements were performed in 50 mM Tris (pH 8), 100 mM NaCl, 25 °C, at a protein concentration of 0.5 μM. Proteolytic cleavage of the linker was induced through addition of Proteinase K to a final concentration of 0.003 U/mL, as previously described.[10,12]

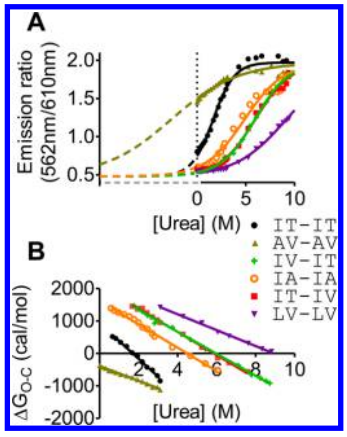

Figure 6. Quantification of the stability of the intramolecular dimer in mOrange−linker−mCherry as mediated by combinations of mutations at the 125 and 127 position. (A) Emission ratio is shown as a function of urea concentration. Data were fit to a Boltzmann distribution. Parameters R_c and R_o were constrained to be the same for all data sets. (B) Plot showing the linear correlation between the urea concentration and the Gibbs free energy associated with transition from the closed to opened state. Data were fit to a linear model and extrapolated to 0 M urea, providing the standard Gibbs free energy of the complex under native conditions (ΔG^0_{o-c}). Measurements were performed in 50 mM Tris (pH 8), 100 mM NaCl, 20 °C, at a protein concentration of 0.5 μM.

M urea, and the high ratio construct having such a weak interaction that only a minor fraction of proteins formed an intramolecular complex at 0 M urea. Because of the lack of a clear plateau phase at low urea concentrations, it would be inaccurate to fit mOr(I125/T127)−linker−mCh(I125/T127) and mOr(A125/V127)−linker−mCh(A125/V127) separately. Given that the group of four constructs displaying a low emission ratio all had a plateau at a similar value, the assumption was made that this starting ratio represented the theoretical minimal emission ratio for all constructs. Consequently, the data in Figure 6A were fit to a Boltzmann distribution (eq 4) where emission ratios associated with the closed and opened states were shared among the entire data set (Table 2). These values, together with the experimental data for each individual data set, were then used to calculate K_x (eq 5) and ΔG^x_{o-c} (eq 6), allowing determination of ΔG^0_{o-c} (eq 7) by extrapolation of the ΔG_{o-c}-urea relation to 0 M urea (Figure 6B). The R125I reversion alone (mOr(I125/T127)−linker−mCh(I125/T127)), previously found to be sufficient to induce a molecular switching-like mechanism in redCALWY-1, introduced a relatively weak stability with ΔG^0_{o-c} = 0.93 kcal/mol (Table 2). An increase in stability (ΔG^0_{o-c} = 1.6 kcal/mol) was achieved by replacement of threonine for alanine at the 127

Table 2. Thermodynamic Parameters of Urea-Induced Dissociation of the mOrange-mCherry Intramolecular Dimer[a]

FP pair	x_0 (M) ± SE	m (kcal/mol/M) ± SE	ΔG^0_{o-c} (kcal/mol) ± SE
IT-IT	1.65 ± 0.02	−0.55 ± 0.02	0.93 ± 0.03
IT-IV	5.96 ± 0.12	−0.36 ± 0.01	2.09 ± 0.03
IV-IT	5.94 ± 0.11	−0.34 ± 0.01	2.02 ± 0.03
LV-LV	9.15 ± 0.17	−0.25 ± 0.01	2.19 ± 0.04
IA-IA	4.87 ± 0.12	−0.36 ± 0.01	1.62 ± 0.04
AV-AV	−2.64 ± 0.46	−0.23 ± 0.01	−0.39 ± 0.01

[a]The fitting procedure constrained parameters R_c (0.48 ± 0.02) and R_o (1.97 ± 0.02) to be the same for all data sets.

dx.doi.org/10.1021/bi500433j | Biochemistry 2014, 53, 6370−6381

position (mOr(I125/A127)−linker−mCh(I125/A127)). Incorporation of the T127V mutation on either of the fluorescent domains further increased that stability to ΔG^0_{o-c} = 2.0 kcal/mol for mOr(I125/V127)−linker−mCh(I125/T127) and ΔG^0_{o-c} = 2.1 kcal/mol for mOr(I125/T127)−linker−mCh(I125/V127). Construct mOr(L125/V127)−linker−mCh(L125/V127) displayed a similar stability with ΔG^0_{o-c} = 2.2 kcal/mol. A ΔG^0_{o-c} of −0.39 kcal/mol was obtained for mOr(A125/V127)−linker−mCh(A125/V127). Please note that this value may be less accurate as it is based on the assumption that the ratio in the closed state is the same as the other variants. Nevertheless, the negative value for ΔG^0_{o-c} confirms that at 0 M urea, a majority of the mOr(A125/V127)−linker−mCh(A125/V127) is in the opened state.

Effect of Dimerization Interface Mutations on Cherry Homodimerization. An alternative method to assess the effects of various interface mutants is to study homodimerization of mCherry as a function of protein concentration using the decrease in fluorescence anisotropy caused by homoFRET.[12,23] Fitting these titration data to a previously described mCherry dimerization model[12] yielded a K_d for dimerization of 33 μM for mCherry(I125/T127), while a much lower K_d of 99 nM was obtained for mCherry(I125/V127) (Figure 7). Data

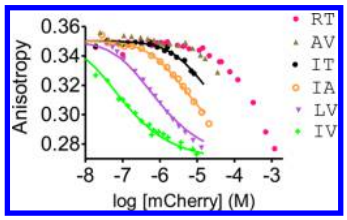

Figure 7. Monitoring mCherry dimerization through homoFRET-induced depolarization. Anistropy was measured as a function of protein concentration in a buffer consisting of 50 mM Tris-HCl (pH 8), 100 mM NaCl, 1 mg/mL BSA, at 25 °C. Data were fit to the same model as described previously,[12] with a high anisotropy level associated with the monomeric state (0.35) and a low anisotropy value associated with the dimeric state (0.27) both constrained in the fitting procedure to be the same for all data sets.

measured at concentrations above 10 μM were not included in the fit, as homoFRET between molecularly dissolved mCherry monomers starts to become significant above this concentration, as was also clearly observed for wild-type mCherry.[12] The mCherry(L125/V127) and mCherry(I125/A127) mutants revealed intermediate K_d's of 0.87 μM and 7.9 μM, respectively (Figure 7). The protein mCherry(A125/V127) only showed an anisotropy decrease at concentrations above 10 μM, which is similar to that observed for wild-type mCherry and is consistent with the finding from the urea-based analysis that this variant's intramolecular complex is very weak. To verify whether the effect of these mutations are similar for mOrange, we also studied studied homodimerization of some variants of mOrange. The Förster distance for mOrange homoFRET is larger than that for mCherry homoFRET (due to the higher quantum yield of mOrange), which makes the determination of relatively weak interactions less reliable, as these are more difficult to distinguish from homoFRET between mOrange monomers at high concentration.[23] This is clearly seen with monomeric mOrange(R125/T127) (Figure S4, Supporting Information), where the decrease in anisotropy starts at a lower concentrations than for monomeric mCherry(R125/T127) (Figure 7). Nevertheless, the dimerization constants obtained for mOrange(I125/T127) of 13 μM and for mOrange(I125/V127) of 31 nM are similar to their mCherry counterparts (Figure S4, Table 3).

Table 3. Homodimer Dissociation Constants for mCherry and mOrange, as Determined by Fluorescence Anisotropy[a]

FP	dimerization K_d (±SE), μM
mCherry-RT	n.a.
mCherry-AV	n.d.
mCherry-IT	33 ± 3
mCherry-IA	7.9 ± 0.5
mCherry-LV	0.87 ± 0.06
mCherry-IV	0.099 ± 0.007
mOrange-IT	13 ± 2
mOrange-IV	0.031 ± 0.005

[a]The fitting procedure constrained parameters R_m (0.35 for mCherry, 0.32 for mOrange) and R_d (0.27 for mCherry, 0.25 for mOrange) to be the same for all data sets.

The fluorescence anisotropy assay results are consistent with the urea titration experiments in regard to the relative strength of the various mutations, with 125I/127V > 125L/127V > 125I/127A > 125I/127T > 125A/127V > 125R/127T. In addition, the effects of mutations at positions 125 and 127 seem to be additive, as the interaction strengths of the mOr(I125/T127)−linker−mCh(I125/V127) and mOr(I125/V127)−linker−mCh(I125/T127) are similar and in between those of the mOr(I125/T127)−linker−mCh(I125/T127) and mOr(I125/V127)−linker−mCh(I125/V127) constructs. The ΔG^0_{o-c} measured for intramolecular complex formation with the urea titration and the K_d for intermolecular dimerization from the fluorescence anisotropy measurements are in principle related. Assuming that the intermolecular homodimer complex is the same as the intramolecular dimer complex, the ΔG^0_{o-c} for the intramolecular interaction is related to the intermolecular K_d by an effective concentration term. This effective concentration (C_{eff}) is determined by the linker length, its flexibility, and the distance that the linker bridges in the complexed state.[35,36] Assuming a distance of 30 Å, a linker length of 81 amino acids and a persistence length of 4.5 Å, C_{eff} can be calculated to be 2.6 mM.[36] On the basis of this value for C_{eff} and $K_{d,inter}$ = 7.9 μM for mCherry(125I/127A), an intramolecular K_d of 0.003 is calculated, which corresponds to a ΔG^0_{o-c} = 3.4 kcal/mol. This value is significantly higher than that obtained directly from the urea titration (1.6 kcal/mol), which is probably because the linker disfavors the formation of the antiparallel dimer structure that is likely to form during intermolecular homodimerization. This finding thus emphasizes the importance of characterizing domain−domain interactions both in an inter- and intramolecular context.

Development of a Red FRET Sensor for Bile Acids Using a Self-Associating mOrange/mCherry FRET Pair. Bile acids are cholesterol-derived steroid molecules that carry out several essential functions in the digestive system and that are also involved in cell signaling.[37] We recently reported the development of a bile acid FRET sensor (BAS-1) based on the ligand-binding domain (LBD) of FXR, a bile-acid regulated nuclear receptor. BAS-1 allowed intracellular imaging of bile acid pools in live cells[16] and was designed based on the principle of mutual exclusive domain interactions. Self-associating variants of Cerulean and Citrine were used that can interact in the absence of bile acid, resulting in a high level

dx.doi.org/10.1021/bi500433j | Biochemistry 2014, 53, 6370−6381

of FRET. Upon binding of bile acid to the ligand binding domain (LBD), an intramolecular interaction between an LXXLL peptide motif and the FXR-LBD coactivator site is formed, which disrupts the interaction between the fluorescent domains and results in a decrease in FRET.[16] The sensor response was shown to critically depend on the intramolecular interaction between the fluorescent domains, since a control sensor with noninteracting, wild-type Cerulean and Citrine did not show a significant change in FRET. To test the interchangeability of self-associating FRET pairs, we replaced the Cerulean and Citrine fluorescent domains in BAS-1 by four different mOrange2[38] and mCherry FRET pairs (Figure 8A and

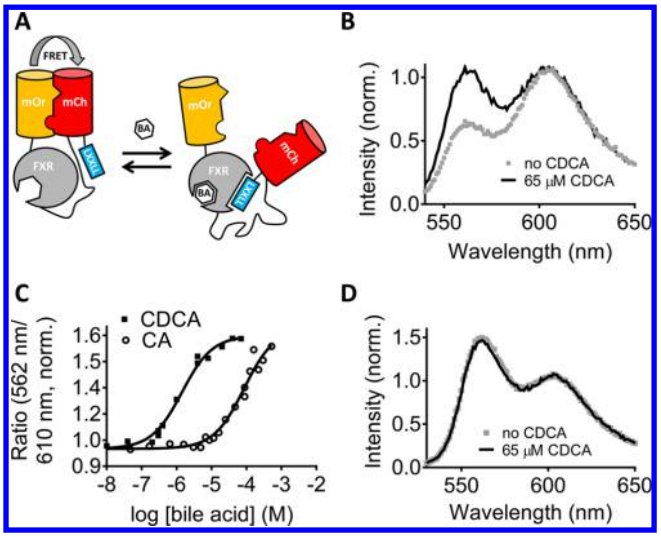

Figure 8. Design and characterization of red-shifted bile acid sensor redBAS-1. (A) Schematic representation of redBAS-1 mechanism of action. In the absence of bile acid (BA), mOrange2 and mCherry form an intramolecular dimer. When bile acid binds to the ligand binding pocket of the FXR-LBD domain, the LXXLL motif directly fused to the mCherry C-terminus binds to the coactivator binding site on FXR-LBD, disrupting the intramolecular mOrange2−mCherry complex. (B) Fluorescence emission spectra of redBAS-1 in the absence and presence of 65 μM CDCA after excitation at 520 nm. Spectra were normalized to the emission at 610 nm. (C) The redBAS-1 fluorescence emission ratio was monitored as a function of CDCA or CA concentration. The emission ratio was normalized to the value obtained in the absence of bile acid (BA) and fit to eq 3 (Methods). (D) Fluorescence emission spectra of redBAS-0 in the absence and presence of 65 μM CDCA after excitation at 520 nm. Measurements were performed in 50 mM Tris-HCl (pH 8), 100 mM NaCl, and 1 mM DTT at 25 °C, at a protein concentration of 0.2 μM.

Figure S5A). The variant with the R125I mutation at both donor and acceptor fluorescent domain (redBAS-1) was the only construct that displayed a robust decrease in FRET in response to CDCA addition. To further characterize the sensor properties of redBAS-1, titration experiments were performed with chenodeoxycholic acid (CDCA) and cholic acid (CA). The emission ratio (mOrange2/mCherry) of 0.62 in the absence of ligand corresponds to a high level of FRET and is thus consistent with an interaction between the fluorescent domains (Figure 8B). Addition of ligand resulted in an increase in the emission ratio to 1.0, which is consistent with (at least partial) disruption of the interaction between mOrange2 and mCherry (Figure 8C). Fitting the emission ratio as a function of bile acid concentration revealed a K_d of 1.4 ± 0.2 μM for CDCA and a K_d of 58 ± 10 μM for CA. These values are very similar to those obtained previously for BAS-1, and for FXR.[16] When the R125I mutation on mOrange and mCherry was reverted (redBAS-0), the sensor showed a high starting emission ratio (1.5, indicating low FRET) and no longer responded to CDCA addition (Figure 2D), confirming the crucial role played by the R125I mutations.

■ DISCUSSION

A combination of biophysical techniques was used to quantify the stability of the intramolecular complexes formed by self-associating fluorescent domains. Urea titrations were introduced as a new approach to study these FP domain interactions in the context of a single fusion protein. The previously reported S208F mutation was found to promote formation of an intramolecular complex between ECFP and EYFP with a stability of 2.0 kcal/mol. Surprisingly, the same mutation mediated a much weaker interaction between Cerulean and Citrine (ΔG^0_{o-c} = 0.62 kcal/mol), which could be attributed to two Cerulean-specific mutations. A detailed characterization of the contributions of amino acids at positions 125 and 127 of the dimerization interface of mOrange and mCherry revealed that preventing Coulomb repulsion coupled with additional hydrophobic interactions was necessary for formation of a stable intramolecular interaction for this red FRET pair. Conformational stabilities ranging from −0.4 to 2.2 kcal/mol were found for the various mOrange−mCherry interface mutations.

The mutations showed the same behavior when assessed by their stabilizing effect on the formation of mCherry homodimers using fluorescence anisotropy. Values for the intramolecular equilibrium constants that were calculated based on these intermolecular K_d's were found to be consistently higher than those determined experimentally with the urea assay. One reason for this may be that the intermolecular complex is a heterodimer, whereas homodimers are studied in the anisotropy measumerements. A more likely explanation is that the linker between the two fluorescent domains disfavors the formation of an antiparallel dimer, which is the complex that is typically found in crystal structures. This could also explain why introduction of a circularly permuted fluorescent domain can substantially increase a FRET-sensor's dynamic range, as circular permutation reverses the relative orientation of fluorescent domains with respect to each other.[17]

When sticky FRET pairs are used in bimolecular assays, for example, to investigate protein−protein interactions (PPIs) or host−guest supramolecular interactions, the interaction between the fused FPs can affect the apparent affinity measured for the interaction of interest.[39,40] The presence of the sticky mutation S208F has been reported to increase the affinity of ECFP-lithocholic acid for EYFP-β-cyclodextrin 10-fold.[41] Interestingly, the latter increase in affinity would indicate the sticky FP interaction contributed ∼1.3 kcal/mol ($\Delta\Delta G$ = $-RT^*$ ln(K_{d1}/K_{d2}) = $-RT^*$ln(0.1)) to the overall binding, close to the value that was obtained for the stability of the ECFP*-L9-EYFP* intramolecular complex (2.0 kcal/mol). Conversely, in single-chain FRET sensors exploiting mutually exclusive conformations, a stabilization of one conformation necessarily entails a free energy penalty for the other. Indeed, several examples in the literature bear out this prediction. The presence of CyPet and YPet in a FRET sensor for peptides weakened the sensor's affinity for peptide 3-fold.[14] Introduction of S208F and V224L into the eCALWY-1 Cerulean/Citrine-based FRET sensor for Zn^{2+} resulted in a 10-fold weakening of

Zn^{2+} affinity.[11] We recently reported that replacing the Cerulean and Citrine domains in eCALWY-1 with mOrange (I125/T127) and mCherry (I125/T127) resulted in a similarly attenuated affinity for Zn^{2+},[12] confirming that the mOrange-(I125/T127)−mCherry(I125I/T127) interaction is comparable in stability to the Cerulean*−Citrine* interaction in eCALWY-1.

Previous work has demonstrated that differing levels of FP complex stability were appropriate for different FRET sensors.[17] Ca^{2+} FRET sensors YC3.60 and TN-XL had the highest DR when the native CFP/YFP interface was used and performed more poorly when either dimerizing mutations were introduced or when the interface was disrupted with the A206K mutation.[42] The YFP acceptors used here were both of the circularly permutated variety, and it was the use of these acceptors that had originally been reported to improve the sensors' DR.[9,43] Kotera et al. speculated that the circular permutation helped juxtapose the FPs in the correct orientation, allowing for an intramolecular interaction in the Ca^{2+}-bound state.[17] Remarkably, it was found that replacement of ECFP with Cerulean negated the enhancing effect of a circularly permutated acceptor in the Ca^{2+} sensor TN-XL.[9] Our finding that Cerulean contains interface destabilizing mutations helps to explain this initially puzzling observation. Similarly, introduction of third generation CFP variants mCerulean3 (with Y145A)[44] and Turquoise2 (with H148D)[45] into the recently developed Twitch Ca^{2+} FRET sensor severely perturbed the sensor's functioning. Extensive screening of linker libraries was required to recover the dynamic range of this sensor.[46] Our results predict that using the recently developed CFP variant Aquamarine (ECFP with T65S and H148G)[47] might be a better choice for replacing CFP in the Twitch sensor, providing enhanced brightness and photostability without perturbing the intramolecular FP-FP interaction.

Recently, two alternative strategies for the construction of fluorescent sensor proteins have been reported that also rely on controlling intramolecular domain interactions. Campbell[48,49] and co-workers introduced weak or nonfluorescent protein monomers that associate to form a heterodimer complex in which one of the domains regains fluorescence. A pair of dTomato variants that form a heterodimeric complex with a K_d of 33 μM was successfully applied to detect protein−protein interactions both in vitro and in situ and was used to construct a caspase-3 sensor. More recently green and yellow variants were introduced that displayed slightly lower values of K_d, which somewhat suppressed the observed dynamic range when used in the context of an intracellular reporter for caspase-3 activity. A second strategy was reported by Serrano and co-workers, who introduced weak peptide−domain interactions based on SH3 or WW domains to enhance FRET between noninteracting fluorescent domains.[50] The peptide−domain interaction was tuned to prevent intermolecular background binding and only occurred when the two proteins of interest that were fused to the FPs formed a complex. This strategy thus allowed physical decoupling of the fluorescence and interaction modules and helped to improve FRET efficiency between evolutionarily unrelated Citrine and mCherry.[50,51] Interestingly, optimal performance was observed using a peptide−domain K_d of 170 μM, which is even weaker than the optimal affinities observed for the self-associating FRET pairs and the dimerization-dependent fluorescent proteins. Since these protein switches also require a balance of intra- and intermolecular domain−domain interactions, progress with these strategies is likely to also benefit from the methods and insights developed in this study.

The red-shifted bile acid sensor redBAS-1 represents the third example, after a sensor for Zn^{2+} and for protease activity,[12] in which the newly found mOrange−mCherry interacting FRET pair proved essential for sensor functioning. A key aspect to these switch-like sensors is the strength of the intramolecular interaction between the fluorescent domains. Introduction of different combinations of the R125I and T127 V mutations into redBAS-1, resulting in redBAS-2, -3, and -4, had been expected to weaken these sensors' affinity for bile acid and to increase the DR. However, the ratiometric responses of redBAS-2, -3, and -4 were all much smaller than the response seen for redBAS-1. We speculate that the increased hydrophobicity of the fluorescent domains' surfaces found in redBAS-2, -3, and -4 may lead to an interaction between FXR-LBD and the fluorescent domains. Nevertheless, the optimal interaction strength found for the mOrange−mCherry interaction (0.93 kCal/mol, with mOr-(I125/T127)−mCh(I125/T127)) closely matches that of counterpart FRET sensors employing Cerulean and Citrine.[11,16,34]

In conclusion, a comprehensive study of the hydrophobic interactions between various self-associating FRET pairs was reported. In addition, a set of mOrange/mCherry FRET pairs has been developed with a broad range of interaction strengths, yielding further understanding of the mOrange−mCherry dimerization interface and the mutations tolerated therein. These findings not only allow a better understanding of the important role of intramolecular domain interactions in many current FRET sensors but also provide a framework for the development of new self-associating FRET pairs, such as derivatives of green and red FPs.[52]

■ ASSOCIATED CONTENT

Supporting Information

Table listing the primers used for site directed mutagenesis, tables listing anisotropy values measured for various Cerulean−linker−Citrine and mOrange−linker−mCherry constructs, the annotated DNA and amino acid sequence for the Cer*(A145Y/D148H)-L9-Cit* and redBAS-1 constructs, a graph indicating the isosbestic point in the Cerulean and Citrine spectra, a graph showing the mOrange anisotropy and a graph of the CDCA titrations with four different redBAS constructs. This material is available free of charge via the Internet at http://pubs.acs.org.

■ AUTHOR INFORMATION

Corresponding Author

*E-mail: m.merkx@tue.nl; phone: ++31-402474728.

Funding

This work was supported by a Vidi grant (700.56.428) from The Netherlands Organization of Scientific Research and an ERC starting grant (ERC-2011-StG 280255).

Notes

The authors declare no competing financial interest.

■ ACKNOWLEDGMENTS

We thank Quincy van Houtum for performing initial urea titration experiments and Dr. Jan Vinkenborg for providing several of the expression plasmids.

REFERENCES

(1) Campbell, R. E. (2009) Fluorescent-protein-based biosensors: modulation of energy transfer as a design principle. *Anal. Chem. 81*, 5972−5979.

(2) Palmer, A. E., Qin, Y., Park, J. G., and McCombs, J. E. (2011) Design and application of genetically encoded biosensors. *Trends Biotechnol. 29*, 144−152.

(3) Frommer, W. B., Davidson, M. W., and Campbell, R. E. (2009) Genetically encoded biosensors based on engineered fluorescent proteins. *Chem. Soc. Rev. 38*, 2833−2841.

(4) Hamers, D., van Voorst Vader, L., Borst, J. W., and Goedhart, J. (2013) Development of FRET biosensors for mammalian and plant systems. *Protoplasma 251*, 333−347.

(5) Merkx, M., Golynskiy, M. V., Lindenburg, L. H., and Vinkenborg, J. L. (2013) Rational design of FRET sensor proteins based on mutually exclusive domain interactions. *Biochem. Soc. Trans. 41*, 1201−1205.

(6) Heim, N., and Griesbeck, O. (2004) Genetically encoded indicators of cellular calcium dynamics based on troponin C and green fluorescent protein. *J. Biol. Chem. 279*, 14280−14286.

(7) Ouyang, M., Huang, H., Shaner, N. C., Remacle, A. G., Shiryaev, S. A., Strongin, A. Y., Tsien, R. Y., and Wang, Y. (2010) Simultaneous visualization of protumorigenic Src and MT1-MMP activities with fluorescence resonance energy transfer. *Cancer Res. 70*, 2204−2212.

(8) Jost, C. A., Reither, G., Hoffmann, C., and Schultz, C. (2008) Contribution of fluorophores to protein kinase C FRET probe performance. *ChemBioChem 9*, 1379−1384.

(9) Mank, M., Reiff, D. F., Heim, N., Friedrich, M. W., Borst, A., and Griesbeck, O. (2006) A FRET-based calcium biosensor with fast signal kinetics and high fluorescence change. *Biophys. J. 90*, 1790−1796.

(10) Vinkenborg, J. L., Evers, T. H., Reulen, S. W., Meijer, E. W., and Merkx, M. (2007) Enhanced sensitivity of FRET-based protease sensors by redesign of the GFP dimerization interface. *ChemBioChem 8*, 1119−1121.

(11) Vinkenborg, J. L., Nicolson, T. J., Bellomo, E. A., Koay, M. S., Rutter, G. A., and Merkx, M. (2009) Genetically encoded FRET sensors to monitor intracellular Zn^{2+} homeostasis. *Nat. Methods 6*, 737−740.

(12) Lindenburg, L. H., Hessels, A. M., Ebberink, E. H., Arts, R., and Merkx, M. (2013) Robust red FRET sensors using self-associating fluorescent domains. *ACS Chem. Biol. 8*, 2133−2139.

(13) Koay, M. S., Janssen, B. M., and Merkx, M. (2013) Tuning the metal binding site specificity of a fluorescent sensor protein: from copper to zinc and back. *Dalton Trans. 42*, 3230−3232.

(14) Huang, J., and Koide, S. (2010) Rational conversion of affinity reagents into label-free sensors for Peptide motifs by designed allostery. *ACS Chem. Biol. 5*, 273−277.

(15) Golynskiy, M. V., Rurup, W. F., and Merkx, M. (2010) Antibody detection by using a FRET-based protein conformational switch. *ChemBioChem 11*, 2264−2267.

(16) van der Velden, L. M., Golynskiy, M. V., Bijsmans, I. T., van Mil, S. W., Klomp, L. W., Merkx, M., and van de Graaf, S. F. (2013) Monitoring bile acid transport in single living cells using a genetically encoded Forster resonance energy transfer sensor. *Hepatology 57*, 740−752.

(17) Kotera, I., Iwasaki, T., Imamura, H., Noji, H., and Nagai, T. (2010) Reversible dimerization of *Aequorea victoria* fluorescent proteins increases the dynamic range of FRET-based indicators. *ACS Chem. Biol. 5*, 215−222.

(18) Evers, T. H., van Dongen, E. M., Faesen, A. C., Meijer, E. W., and Merkx, M. (2006) Quantitative understanding of the energy transfer between fluorescent proteins connected via flexible peptide linkers. *Biochemistry 45*, 13183−13192.

(19) Quan, J., and Tian, J. (2009) Circular polymerase extension cloning of complex gene libraries and pathways. *PLoS One 4*, e6441.

(20) Nagai, T., Ibata, K., Park, E. S., Kubota, M., Mikoshiba, K., and Miyawaki, A. (2002) A variant of yellow fluorescent protein with fast and efficient maturation for cell-biological applications. *Nat. Biotechnol. 20*, 87−90.

(21) Griesbeck, O., Baird, G. S., Campbell, R. E., Zacharias, D. A., and Tsien, R. Y. (2001) Reducing the environmental sensitivity of yellow fluorescent protein. *J. Biol. Chem. 276*, 29188−29194.

(22) Shaner, N. C., Campbell, R. E., Steinbach, P. A., Giepmans, B. N., Palmer, A. E., and Tsien, R. Y. (2004) Improved monomeric red, orange and yellow fluorescent proteins derived from *Discosoma* sp. red fluorescent protein. *Nat. Biotechnol. 22*, 1567−1572.

(23) Espagne, A., Erard, M., Madiona, K., Derrien, V., Jonasson, G., Levy, B., Pasquier, H., Melki, R., and Merola, F. (2011) Cyan fluorescent protein carries a constitutive mutation that prevents its dimerization. *Biochemistry 50*, 437−439.

(24) Nguyen, A. W., and Daugherty, P. S. (2005) Evolutionary optimization of fluorescent proteins for intracellular FRET. *Nat. Biotechnol. 23*, 355−360.

(25) Stepanenko, O. V., Kuznetsova, I. M., Verkhusha, V. V., and Turoverov, K. K. (2013) Beta-barrel scaffold of fluorescent proteins: folding, stability and role in chromophore formation. *Int. Rev. Cell Mol. Biol. 302*, 221−278.

(26) Pomorski, A., Kochanczyk, T., Miloch, A., and Krezel, A. (2013) Method for accurate determination of dissociation constants of optical ratiometric systems: chemical probes, genetically encoded sensors, and interacting molecules. *Anal. Chem. 85*, 11479−11486.

(27) Zhou, H. X. (2001) The affinity-enhancing roles of flexible linkers in two-domain DNA-binding proteins. *Biochemistry 40*, 15069−15073.

(28) Möglich, A., Joder, K., and Kiefhaber, T. (2006) End-to-end distance distributions and intrachain diffusion constants in unfolded polypeptide chains indicate intramolecular hydrogen bond formation. *Proc. Natl. Acad. Sci. U. S. A. 103*, 12394−12399.

(29) Soranno, A., Longhi, R., Bellini, T., and Buscaglia, M. (2009) Kinetics of contact formation and end-to-end distance distributions of swollen disordered peptides. *Biophys. J. 96*, 1515−1528.

(30) Pace, C. N., Huyghues-Despointes, B. M., Fu, H., Takano, K., Scholtz, J. M., and Grimsley, G. R. (2010) Urea denatured state ensembles contain extensive secondary structure that is increased in hydrophobic proteins. *Protein Sci. 19*, 929−943.

(31) Stepanenko, O. V., Kuznetsova, I. M., Verkhusha, V. V., Staiano, M., D'Auria, S., and Turoverov, K. K. (2010) Denaturation of proteins with beta-barrel topology induced by guanidine hydrochloride. *Spectroscopy 24*, 367−373.

(32) Rizzo, M. A., Springer, G. H., Granada, B., and Piston, D. W. (2004) An improved cyan fluorescent protein variant useful for FRET. *Nat. Biotechnol. 22*, 445−449.

(33) Lelimousin, M., Noirclerc-Savoye, M., Lazareno-Saez, C., Paetzold, B., Le Vot, S., Chazal, R., Macheboeuf, P., Field, M. J., Bourgeois, D., and Royant, A. (2009) Intrinsic dynamics in ECFP and Cerulean control fluorescence quantum yield. *Biochemistry 48*, 10038−10046.

(34) Golynskiy, M. V., Rurup, W. F., and Merkx, M. (2010) Antibody detection by using a FRET-based protein conformational switch. *ChemBioChem 11*, 2264−2267.

(35) van Dongen, E. M., Evers, T. H., Dekkers, L. M., Meijer, E. W., Klomp, L. W., and Merkx, M. (2007) Variation of linker length in ratiometric fluorescent sensor proteins allows rational tuning of Zn(II) affinity in the picomolar to femtomolar range. *J. Am. Chem. Soc. 129*, 3494−3495.

(36) Evers, T. H., Appelhof, M. A., de Graaf-Heuvelmans, P. T., Meijer, E. W., and Merkx, M. (2007) Ratiometric detection of Zn(II) using chelating fluorescent protein chimeras. *J. Mol. Biol. 374*, 411−425.

(37) de Aguiar Vallim TQ, T. E., and Edwards, P. A. (2013) Pleiotropic roles of bile acids in metabolism. *Cell Metab. 17*, 657−669.

(38) Shaner, N. C., Lin, M. Z., McKeown, M. R., Steinbach, P. A., Hazelwood, K. L., Davidson, M. W., and Tsien, R. Y. (2008) Improving the photostability of bright monomeric orange and red fluorescent proteins. *Nat. Methods 5*, 545−551.

(39) You, X., Nguyen, A. W., Jabaiah, A., Sheff, M. A., Thorn, K. S., and Daugherty, P. S. (2006) Intracellular protein interaction mapping with FRET hybrids. *Proc. Natl. Acad. Sci. U. S. A. 103*, 18458−18463.

(40) Ohashi, T., Galiacy, S. D., Briscoe, G., and Erickson, H. P. (2007) An experimental study of GFP-based FRET, with application to intrinsically unstructured proteins. *Protein Sci. 16*, 1429−1438.
(41) Uhlenheuer, D. A., Wasserberg, D., Nguyen, H., Zhang, L., Blum, C., Subramaniam, V., and Brunsveld, L. (2009) Modulation of protein dimerization by a supramolecular host-guest system. *Chemistry 15*, 8779−8790.
(42) Zacharias, D. A., Violin, J. D., Newton, A. C., and Tsien, R. Y. (2002) Partitioning of lipid-modified monomeric GFPs into membrane microdomains of live cells. *Science 296*, 913−916.
(43) Nagai, T., Yamada, S., Tominaga, T., Ichikawa, M., and Miyawaki, A. (2004) Expanded dynamic range of fluorescent indicators for Ca^{2+} by circularly permuted yellow fluorescent proteins. *Proc. Natl. Acad. Sci. U. S. A. 101*, 10554−10559.
(44) Markwardt, M. L., Kremers, G. J., Kraft, C. A., Ray, K., Cranfill, P. J., Wilson, K. A., Day, R. N., Wachter, R. M., Davidson, M. W., and Rizzo, M. A. (2011) An improved Cerulean fluorescent protein with enhanced brightness and reduced reversible photoswitching. *PLoS One 6*, e17896.
(45) Goedhart, J., von Stetten, D., Noirclerc-Savoye, M., Lelimousin, M., Joosen, L., Hink, M. A., van Weeren, L., Gadella, T. W., Jr., and Royant, A. (2012) Structure-guided evolution of cyan fluorescent proteins towards a quantum yield of 93%. *Nat. Commun. 3*, 751.
(46) Thestrup, T., Litzlbauer, J., Bartholomaus, I., Mues, M., Russo, L., Dana, H., Kovalchuk, Y., Liang, Y., Kalamakis, G., Laukat, Y., Becker, S., Witte, G., Geiger, A., Allen, T., Rome, L. C., Chen, T. W., Kim, D. S., Garaschuk, O., Griesinger, C., and Griesbeck, O. (2014) Optimized ratiometric calcium sensors for functional in vivo imaging of neurons and T lymphocytes. *Nat. Methods 11*, 175−182.
(47) Erard, M., Fredj, A., Pasquier, H., Beltolngar, D. B., Bousmah, Y., Derrien, V., Vincent, P., and Merola, F. (2013) Minimum set of mutations needed to optimize cyan fluorescent proteins for live cell imaging. *Mol. Biosyst. 9*, 258−267.
(48) Alford, S. C., Abdelfattah, A. S., Ding, Y. D., and Campbell, R. E. (2012) A fluorogenic red fluorescent protein heterodimer. *Chem. Biol. 19*, 353−360.
(49) Alford, S. C., Ding, Y. D., Simmen, T., and Campbell, R. E. (2012) Dimerization-dependent green and yellow fluorescent proteins. *ACS Synth. Biol. 1*, 569−575.
(50) Grünberg, R., Burnier, J. V., Ferrar, T., Beltran-Sastre, V., Stricher, F., van der Sloot, A. M., Garcia-Olivas, R., Mallabiabarrena, A., Sanjuan, X., Zimmermann, T., and Serrano, L. (2013) Engineering of weak helper interactions for high-efficiency FRET probes. *Nat. Methods 10*, 1021−1027.
(51) Jalink, K. (2013) hiFRET: some tailwind for FRET resolves weak protein interactions. *Nat. Methods 10*, 947−948.
(52) Lam, A. J., St-Pierre, F., Gong, Y., Marshall, J. D., Cranfill, P. J., Baird, M. A., McKeown, M. R., Wiedenmann, J., Davidson, M. W., Schnitzer, M. J., Tsien, R. Y., and Lin, M. Z. (2012) Improving FRET dynamic range with bright green and red fluorescent proteins. *Nat. Methods 9*, 1005−1012.